

# A NEW METHOD FOR INVERSE ELECTROMAGNETIC CASTING PROBLEMS BASED ON THE TOPOLOGICAL DERIVATIVE

ALFREDO CANELAS, ANTONIO A. NOVOTNY, AND JEAN R. ROCHE

ABSTRACT. The inverse electromagnetic casting problem consists in looking for a suitable set of electric wires such that the electromagnetic field induced by an alternating current passing through them makes a given mass of liquid metal acquire a predefined shape. In this paper we propose a new method for the topology design of such inductors. The inverse electromagnetic casting problem is formulated as an optimization problem, and topological derivatives are considered in order to locate new wires in the right position. Several numerical examples are presented showing that the proposed technique is effective to design suitable inductors.

## 1. INTRODUCTION

The industrial technique of electromagnetic casting allows for contactless heating, shaping and controlling of chemical aggressive, hot melts. The main advantage over the conventional crucible shape forming is that the liquid metal does not come into contact with the crucible wall, so there is no danger of contamination. This is very important in the preparation of very pure specimens in metallurgical experiments, as even small traces of impurities, such as carbon and sulphur, can affect the physical properties of the sample. Industrial applications are, for example, electromagnetic shaping of aluminum ingots using soft-contact confinement of the liquid metal, electromagnetic shaping of components of aeronautical engines made of superalloy materials (Ni, Ti, . . .), control of the structure solidification, etc. [62, 25].

The electromagnetic casting is based on the repulsive forces that an electromagnetic field produces on the surface of a mass of liquid metal. In the presence of an induced electromagnetic field, the liquid metal changes its shape until an equilibrium relation between the electromagnetic pressure and the surface tension is satisfied. The direct problem in electromagnetic casting consists in determining the equilibrium shape of the liquid metal. In general, this problem can be solved either directly studying the equilibrium equation defined on the surface of the liquid metal, or minimizing an appropriate energy functional. The main advantage of this last method is that the resulting shapes are mechanically stable [41, 56, 29].

The inverse problem consists in determining the electric currents and the induced exterior field, for which the liquid metal takes on a given desired shape. This is a very important problem that one needs to solve in order to define a process of electromagnetic liquid metal forming.

In a previous work we studied the inverse electromagnetic casting problem considering the case where the inductors are made of single solid-core wires with a negligible area of the cross-section [17]. In a second paper we considered the more realistic case where each inductor is a set of bundled insulated strands [16]. In both cases the number of inductors was fixed in advance. In this paper we aim to overcome this constraint, and look for configurations of inductors considering different topologies with the purpose of obtaining better results. In order to manage this new situation we introduce a new formulation for the inverse problem using a shape functional based on the Kohn-Vogelius criterion, see [55, 24, 37, 14, 20]. A topology optimization procedure is defined by means of topological derivatives.

The remaining contents of this paper are organized as follows. The next section describes the direct free-surface problem concerning the electromagnetic casting. Section 3 introduces

---

*Key words and phrases.* Topological asymptotic analysis, topological derivatives, inverse problem, electromagnetic casting.

the topological derivative concept. Section 4 presents the inverse problem in electromagnetic casting, describes how to formulate this problem as an optimization problem, and shows how to compute the topological derivative of the objective functional. The numerical method proposed here to construct the solution using the topological derivative is detailed in Section 5. Some examples are presented in Section 6 to show the efficacy of the proposed approach. Finally, the conclusions of this paper are presented in Section 7.

## 2. THE MATHEMATICAL MODEL OF THE ELECTROMAGNETIC CASTING PROBLEM

The simplified model of the electromagnetic casting problem studied here concerns the case of a vertical column of liquid metal falling down into an electromagnetic field created by vertical inductors. We assume that the frequency of the imposed current is very high so that the magnetic field does not penetrate into the metal. In other words, we neglect the skin effect. Moreover, we assume that a stationary horizontal section is reached so that the 2-dimensional model is valid. The equilibrium of the system is ensured by the static balance on the surface of the metal between the surface tension and the electromagnetic forces. This problem and other similar ones have been considered by several authors, we refer the reader to the following papers for the physical analysis of the simplifying assumptions of the model: see [11, 26, 30, 41, 49, 51, 56].

We denote by  $\Omega \subset \mathbb{R}^2$  the exterior of the closed and simply connected domain  $\omega$  occupied by the cross-section of the metal column. The exterior magnetic field can be found as the solution of the following boundary value problem:

$$\begin{cases} \nabla \times \mathbf{B} = \mu_0 \mathbf{J} & \text{in } \Omega, \\ \nabla \cdot \mathbf{B} = 0 & \text{in } \Omega, \\ \mathbf{B} \cdot \mathbf{n} = 0 & \text{on } \Gamma, \\ \|\mathbf{B}(x)\| = O(\|x\|^{-1}) \text{ as } \|x\| \rightarrow \infty & \text{in } \Omega. \end{cases} \quad (1)$$

Here the fields  $\mathbf{J} = (0, 0, j_0)$  and  $\mathbf{B} = (B_1, B_2, 0)$  represent the mean square values of the current density vector and the total magnetic field, respectively. The constant  $\mu_0$  is the vacuum permeability,  $\mathbf{n}$  the unit normal vector to the boundary  $\Gamma$  of  $\Omega$  and  $\|\cdot\|$  denotes the Euclidean norm. We assume that  $j_0$  has compact support in  $\Omega$  and satisfies:

$$\int_{\Omega} j_0 \, dx = 0. \quad (2)$$

Besides, the cross-section area of the liquid metal column is known and equal to  $S_0$ :

$$\int_{\omega} dx = S_0. \quad (3)$$

The magnetic field produces a surface pressure that acts on the liquid metal changing its shape until the equilibrium is attained. The equilibrium is characterized by the following equation [51, 52, 53, 54, 50]:

$$\frac{1}{2\mu_0} \|\mathbf{B}\|^2 + \sigma \mathcal{C} = p_0 \quad \text{on } \Gamma, \quad (4)$$

where  $\mathcal{C}$  is the curvature of  $\Gamma$  seen from the metal,  $\sigma$  is the surface tension of the liquid and the constant  $p_0$  is an unknown of the problem. Physically,  $p_0$  represents the difference between the internal and external pressures.

In the direct problem the electric current density  $j_0$  is given and one needs to find the shape of  $\omega$  that satisfies (3) and such that the magnetic field  $\mathbf{B}$  solution of (1) satisfies also the equilibrium equation (4) for a real constant  $p_0$ .

Conditions (1) and (2), with the function  $j_0$  compactly supported in  $\Omega$ , imply the existence of the flux function  $\varphi : \Omega \rightarrow \mathbb{R}$  such that  $\mathbf{B} = (\frac{\partial \varphi}{\partial x_2}, -\frac{\partial \varphi}{\partial x_1}, 0)$ , with  $\varphi$  solution of:

$$\begin{cases} -\Delta \varphi = \mu_0 j_0 & \text{in } \Omega, \\ \varphi = 0 & \text{on } \Gamma, \\ \varphi(x) = c + o(1) & \text{as } \|x\| \rightarrow \infty. \end{cases} \quad (5)$$

This equation have a unique solution in the space  $W_0^1(\Omega)$  defined as [46]:

$$W_0^1(\Omega) = \{u : \rho u \in L^2(\Omega) \text{ and } \nabla u \in L^2(\Omega)\}, \quad (6)$$

with  $\rho(x) = [\sqrt{1 + \|x\|^2} \log(2 + \|x\|^2)]^{-1}$ . The constant  $c$  of the condition at infinity in (5) is also an unknown, which has a unique solution in  $\mathbb{R}$ . Equivalent formulations of the conditions at infinity are  $\varphi(x) = O(1)$  and  $\varphi(x) = c + O(1/\|x\|)$  [8]. The form used in (5) is the most convenient in the development of numerical methods of solution.

The solution  $\varphi$  of the exterior problem (5) satisfies the following Poincaré type inequality: there exist a constant  $C > 0$  such that [46]

$$\|\varphi\|_{W_0^1(\Omega)} \leq C \|\nabla \varphi\|_{L^2(\Omega)}, \quad (7)$$

where the norm  $\|\cdot\|_{W_0^1(\Omega)}$  comes from the scalar product of the Hilbert space  $W_0^1(\Omega)$ :

$$\langle u, v \rangle_{W_0^1(\Omega)} = \int_{\Omega} \nabla u \cdot \nabla v \, dx + \int_{\Omega} \rho^2 u v \, dx. \quad (8)$$

The equilibrium equation (4) in terms of the flux becomes:

$$\frac{1}{2\mu_0} \left| \frac{\partial \varphi}{\partial n} \right|^2 + \sigma \mathcal{C} = p_0 \quad \text{on } \Gamma. \quad (9)$$

The direct problem, in terms of the flux, consists in looking for a domain  $\omega$  such that the solution  $\varphi$  of (5) satisfies (9) for a real constant  $p_0$ .

### 3. TOPOLOGICAL DERIVATIVE CONCEPT

The topological derivative measures the sensitivity of a given shape functional with respect to an infinitesimal singular domain perturbation, such as the insertion of holes, inclusions, source-terms or even cracks. The topological derivative was rigorously introduced by Sokołowski and Żochowski [57]. Since then, this concept has proved extremely useful in the treatment of a wide range of problems, namely, topology optimization [1, 3, 4, 7, 15, 48], inverse analysis [5, 21, 28, 32, 40] and image processing [9, 10, 31, 33, 38], and has become a subject of intensive research. Concerning the theoretical development of the topological asymptotic analysis, the reader may refer to the papers [2, 6, 18, 23, 27, 34, 36, 39, 42, 43, 44, 45, 58, 59], for instance.

More precisely, let us consider that the domain  $\Omega$  is subject to a non-smooth perturbation confined in a small ball  $B_\varepsilon(\hat{x})$  of radius  $\varepsilon$  and center  $\hat{x} \in \Omega$ . Then, we assume that a given shape functional  $\psi(\varepsilon)$ , associated to the topologically perturbed domain, admits the following topological asymptotic expansion [57]

$$\psi(\varepsilon) = \psi(0) + f(\varepsilon) D_T \psi + o(f(\varepsilon)), \quad (10)$$

where  $\psi(0)$  is the shape functional associated to the original (unperturbed) domain and  $f(\varepsilon)$  is a positive function such that  $f(\varepsilon) \rightarrow 0$ , when  $\varepsilon \rightarrow 0$ . The function  $\hat{x} \mapsto D_T \psi(\hat{x})$  is called the topological derivative of  $\psi$  at  $\hat{x}$ . Therefore, this derivative can be seen as a first order correction of  $\psi(0)$  to approximate  $\psi(\varepsilon)$ . In fact, the topological derivative  $D_T \psi$  is a scalar function defined over the original domain that indicates, at each point, the sensitivity of the shape functional when a singular perturbation of size  $\varepsilon$  is introduced at that point.

In this paper we propose a new method for inverse electromagnetic casting problems based on the topological asymptotic expansion (10), which is presented in details in the next section.

### 4. THE INVERSE PROBLEM

The goal of the inverse problem is to find a distribution of current around the liquid metal column so that it attains a given shape. Therefore, we have to determine the electric current  $j_0$  such that the solution  $\mathbf{B}$  of (1) satisfies also the equilibrium equation (4). This topic has been already studied and there are a few number of papers about the existence of solutions of the inverse problem, see [30, 22]. Although these above-mentioned references constitute an important insight on the existence issue, we are also interested in obtaining approximate

solutions in situations where the existence of solutions can not be ensured. In other words, if the inverse problem has a solution, we say that the target shape is shapable, if it does not, we say that it is not shapable. In the last case we will be interested in obtaining a distribution  $j_0$  such that the equilibrium shape be a good approximate to the target shape. There are also two other reasons that lead us to reject the idea of an algorithm for obtaining exact solutions only. First, to the author's knowledge, there is not a complete treatise about the characterization of the solution set, and, considering a shapable shape, the uniqueness of the solution in terms of  $j_0$  can not be ensured. Second, unlike the direct problem, the inverse problem is inherently ill posed: small variation of the liquid boundary may cause dramatic variations in the solution  $j_0$  of the inverse problem [30, 22].

These reasons motivates us to formulate the inverse problem as an optimization problem, in order to look for a solution (maybe just approximate solution) minimizing an appropriate functional. There are, however, some known facts about the exact solutions of the inverse problem that are of main importance in what follows. It has been shown [30] that, assuming that the solution  $j_0$  has a compact support, the magnetic field  $\mathbf{B}$  is, in a neighborhood of  $\Gamma$ , the unique analytic extension of the field  $\mathbf{B}\cdot\tau$  defined on the boundary  $\Gamma$  of the liquid metal ( $\tau$  being the unit tangent vector to  $\Gamma$ ). In [30], the authors proved that such analytic extension, solution of (1) and (4), exists only if  $\Gamma$  is an analytic curve, and the function  $\mathbf{B}\cdot\tau$  is analytic. Furthermore, from (4) it is possible to show the following:

$$\mathbf{B}\cdot\tau = \varkappa\sqrt{2\mu_0(p_0 - \sigma\mathcal{C})} \quad \text{with} \quad \varkappa = \pm 1. \quad (11)$$

The constant  $p_0$  must satisfy  $p_0 \geq \max_{\Gamma} \sigma\mathcal{C}$ . If  $p_0 > \max_{\Gamma} \sigma\mathcal{C}$  then  $\varkappa$  should be constant on  $\Gamma$ . That situation is not possible if (2) is satisfied, see [30]. Hence we have the important result:

$$p_0 = \max_{\Gamma} \sigma\mathcal{C}. \quad (12)$$

Another restriction is imposed on  $\Gamma$  since  $\varkappa$  may change the sign at points where  $\mathbf{B}\cdot\tau = 0$  (i.e. where  $\mathcal{C}$  attains its global maximum), depending on the multiplicity order of these zero points: if the multiplicity order of a zero point is even,  $\varkappa$  remains constant. On the other hand, if the multiplicity order of a zero point is odd,  $\varkappa$  changes the sign. Hence, by the periodicity of  $\varkappa$ , the number of zero points of odd order must be even. For example, any curve which has the curvature attaining its maximum value at an odd number of points (at which  $\mathbf{B}\cdot\tau$  has non-degenerate zeros), is in fact impossible to form.

Therefore, calling  $\bar{p} = \sqrt{2\mu_0(p_0 - \sigma\mathcal{C})}$ , with  $p_0$  known and given by (12), the equilibrium constraint in terms of the flux function reads

$$\frac{\partial\varphi}{\partial n} = \varkappa\bar{p} \quad \text{on } \Gamma, \quad (13)$$

where  $\varkappa = \pm 1$ , with the sign changes located at points where the curvature of  $\Gamma$  is a global maximum. Of course we have two possible ways to define  $\varkappa$ . However, both lead to the same solution  $j_0$  but with the opposite sign.

**4.1. Problem Formulation.** The previous considerations allow us to formulate the inverse problem as follows: determine the electric current density  $j_0$  and the real constant  $c$  such that the system

$$\begin{cases} -\Delta\varphi = \mu_0 j_0 & \text{in } \Omega, \\ \varphi = 0 & \text{on } \Gamma, \\ \frac{\partial\varphi}{\partial n} = \varkappa\bar{p} & \text{on } \Gamma, \\ \varphi(x) = c + o(1) & \text{as } \|x\| \rightarrow \infty, \end{cases} \quad (14)$$

has a solution  $\varphi \in W_0^1(\Omega)$ . Let us introduce a shape functional based on the Kohn-Vogelius criterion, namely

$$\psi(0) = J(\phi) = \frac{1}{2}\|\phi\|_{L^2(\Gamma)}^2 = \frac{1}{2}\int_{\Gamma} |\phi|^2 ds, \quad (15)$$

where the auxiliary function  $\phi$  depends implicitly on  $j_0$  and  $c$  by solving the following boundary-value problem

$$\begin{cases} -\Delta\phi = \mu_0 j_0 & \text{in } \Omega, \\ \frac{\partial\phi}{\partial n} = \varkappa \bar{p} & \text{on } \Gamma, \\ \phi(x) = c + o(1) & \text{as } \|x\| \rightarrow \infty. \end{cases} \quad (16)$$

Note that (16) has a unique solution in  $W_0^1(\Omega)$  if and only if the compatibility condition:

$$\int_{\Gamma} \varkappa \bar{p} ds = 0, \quad (17)$$

is satisfied [8, 35].

The approach proposed here to deal with (14) is the following: determine the electric current density  $j_0$  and the constant  $c$  such that the solution  $\phi$  of (16) minimizes the shape functional (15). We note that the minimum of the shape functional (15) is attained when  $\phi \equiv 0$  on  $\Gamma$ . This means that in this situation, from the well-posedness of problems (5) and (16), we have  $\phi \equiv \varphi$  in  $\Omega$ .

In a first step we can eliminate the variable  $c$  of the optimization problem defining it as the global minimum  $c^*(j_0)$  of (15) for any fixed  $j_0$ , i.e., we take  $c = c^*(j_0) = \arg \min_c J(\phi(j_0, c))$ . In fact,  $\phi = \zeta + c$ , where  $\zeta$  is the unique solution in  $W_0^1(\Omega)$  to the following problem

$$\begin{cases} -\Delta\zeta = \mu_0 j_0 & \text{in } \Omega, \\ \frac{\partial\zeta}{\partial n} = \varkappa \bar{p} & \text{on } \Gamma, \\ \zeta(x) = o(1) & \text{as } \|x\| \rightarrow \infty. \end{cases} \quad (18)$$

From (15), and denoting  $|\Gamma| = \int_{\Gamma} ds$ , we have  $J(\phi) = J(\zeta) + c \int_{\Gamma} \zeta ds + \frac{1}{2}c^2|\Gamma|$ . Differentiating this expression with respect to  $c$ , we obtain the global minimum

$$c^*(j_0) = -|\Gamma|^{-1} \int_{\Gamma} \zeta ds. \quad (19)$$

Note also that  $c = c^*(j_0)$  if and only if the integral of  $\phi$  on  $\Gamma$  vanishes. In fact, taking  $c = c^*(j_0)$  we have  $\int_{\Gamma} \phi ds = \int_{\Gamma} \zeta ds + c^*(j_0)|\Gamma| = 0$ . Conversely, if we ask for the integral of  $\phi$  on  $\Gamma$  to be zero, we have  $\int_{\Gamma} \zeta ds + c|\Gamma| = 0$ , that has the solution  $c = c^*(j_0)$ .

Hence, we can formulate an equivalent optimization problem as follows: minimize the shape functional (15), where  $\phi$  depends implicitly on  $j_0$  only, by solving the following problem

$$\begin{cases} -\Delta\phi = \mu_0 j_0 & \text{in } \Omega, \\ \frac{\partial\phi}{\partial n} = \varkappa \bar{p} & \text{on } \Gamma, \\ \int_{\Gamma} \phi ds = 0. \end{cases} \quad (20)$$

The variational formulation of (20) is

$$\phi \in U : \int_{\Omega} \nabla\phi \cdot \nabla\eta dx = \int_{\Gamma} \varkappa \bar{p} \eta ds + \int_{\Omega} \mu_0 j_0 \eta dx \quad \forall \eta \in U, \quad (21)$$

where  $U$  is the closed subspace of  $W_0^1(\Omega)$  defined as  $U = \{u \in W_0^1(\Omega) : \int_{\Gamma} u ds = 0\}$ .

Therefore, the proposed approach is to solve the optimization problem

$$\min_{j_0} \frac{1}{2} \|\phi\|_{L^2(\Gamma)}^2, \quad (22)$$

subject to the constraint given by (21).

Before continue, let us introduce an adjoint state  $v$  for further simplification, which is solution to the following boundary-value problem

$$\begin{cases} -\Delta v = 0 & \text{in } \Omega, \\ \frac{\partial v}{\partial n} = -\phi & \text{on } \Gamma, \\ \int_{\Gamma} v ds = 0. \end{cases} \quad (23)$$

or, equivalently, solution to the variational problem

$$v \in U : \int_{\Omega} \nabla v \cdot \nabla \eta dx + \int_{\Gamma} \phi \eta ds = 0 \quad \forall \eta \in U. \quad (24)$$

Note that the compatibility condition for (23) is satisfied, since the integral of  $\phi$  on  $\Gamma$  vanishes. Hence (23) and (24) always have a unique solution. In addition, we can also split the solution  $v = w + \beta$ , where  $w$  is the unique solution in  $W_0^1(\Omega)$  to the following problem

$$\begin{cases} -\Delta w = 0 & \text{in } \Omega, \\ \frac{\partial w}{\partial n} = -\phi & \text{on } \Gamma, \\ w(x) = o(1) & \text{as } \|x\| \rightarrow \infty, \end{cases} \quad (25)$$

and the constant  $\beta = -|\Gamma|^{-1} \int_{\Gamma} w ds$ .

**4.2. The topological derivative calculation.** Associated to  $\phi$  we define the function  $\phi_\varepsilon$  solution to the perturbed variational problem. In this context, the perturbation is characterized by changing the electric current distribution  $j_0$  by a new one  $j_\varepsilon$  which is identical to  $j_0$  everywhere in  $\Omega$  except in two small regions  $B_\varepsilon(x^+) \subset \Omega$  and  $B_\varepsilon(x^-) \subset \Omega$ , such that  $B_\varepsilon(x^-) \cap B_\varepsilon(x^+) = \emptyset$ . More precisely,  $j_\varepsilon$  is given by

$$j_\varepsilon = j_0 + I\chi_{B_\varepsilon(x^+)} - I\chi_{B_\varepsilon(x^-)}. \quad (26)$$

Therefore, the perturbed electric current distribution  $j_\varepsilon$  also satisfies the compatibility condition (2), namely

$$\int_{\Omega} j_\varepsilon dx = 0. \quad (27)$$

In this way, the shape functional associated to the perturbed problem reads:

$$\psi(\varepsilon) = J(\phi_\varepsilon) = \frac{1}{2} \int_{\Gamma} |\phi_\varepsilon|^2 ds, \quad (28)$$

where  $\phi_\varepsilon$  is solution to the following variational problem:

$$\phi_\varepsilon \in U : \int_{\Omega} \nabla \phi_\varepsilon \cdot \nabla \eta dx = \int_{\Gamma} \varkappa \bar{p} \eta ds + \int_{\Omega} \mu_0 j_\varepsilon \eta dx \quad \forall \eta \in U. \quad (29)$$

Before proceeding, let us introduce the adjoint state  $v_\varepsilon$  associated to the perturbed problem, which is solution to the variational problem

$$v_\varepsilon \in U : \int_{\Omega} \nabla v_\varepsilon \cdot \nabla \eta dx + \int_{\Gamma} \phi_\varepsilon \eta ds = 0 \quad \forall \eta \in U. \quad (30)$$

**Lemma 1.** *Let  $\phi$  and  $\phi_\varepsilon$  be the solutions to the variational problems (21) and (29), respectively. Then, there exist a constant  $C$ , independent of  $\varepsilon$ , such that the inequality*

$$\|\phi_\varepsilon - \phi\|_{W_0^1(\Omega)} \leq C\varepsilon, \quad (31)$$

*is satisfied for any small parameter  $\varepsilon$ .*

*Proof.* We have seen that  $\phi = \zeta + c$  with  $\zeta$  solution to (18) or, equivalently, solution to the variational problem

$$\zeta \in V : \int_{\Omega} \nabla \zeta \cdot \nabla \eta \, dx = \int_{\Gamma} \varkappa \bar{p} \eta \, ds + \int_{\Omega} \mu_0 j_0 \eta \, dx \quad \forall \eta \in V, \quad (32)$$

where  $V = \{u \in W_0^1(\Omega) : u(x) \rightarrow 0 \text{ as } \|x\| \rightarrow \infty\}$  and the constant  $c = -|\Gamma|^{-1} \int_{\Gamma} \zeta \, ds$ . Analogously,  $\phi_\varepsilon = \zeta_\varepsilon + c_\varepsilon$  with  $\zeta_\varepsilon$  solution to the variational problem

$$\zeta_\varepsilon \in V : \int_{\Omega} \nabla \zeta_\varepsilon \cdot \nabla \eta \, dx = \int_{\Gamma} \varkappa \bar{p} \eta \, ds + \int_{\Omega} \mu_0 j_\varepsilon \eta \, dx \quad \forall \eta \in V, \quad (33)$$

and with the constant  $c_\varepsilon = -|\Gamma|^{-1} \int_{\Gamma} \zeta_\varepsilon \, ds$ . By subtracting the variational problems (32) and (33), we get

$$\int_{\Omega} \nabla(\zeta_\varepsilon - \zeta) \cdot \nabla \eta \, dx = \mu_0 I \left( \int_{B_\varepsilon(x^+)} \eta \, dx - \int_{B_\varepsilon(x^-)} \eta \, dx \right) \quad \forall \eta \in V, \quad (34)$$

Now, by taking  $\eta = \zeta_\varepsilon - \zeta$ , we have

$$\int_{\Omega} \|\nabla(\zeta_\varepsilon - \zeta)\|^2 \, dx = \mu_0 I \left( \int_{B_\varepsilon(x^+)} (\zeta_\varepsilon - \zeta) \, dx - \int_{B_\varepsilon(x^-)} (\zeta_\varepsilon - \zeta) \, dx \right). \quad (35)$$

Thanks to the behavior of  $(\zeta_\varepsilon - \zeta)$  at infinity, there exist a constant  $C_1$  such that the following Poincaré type inequality holds [46]

$$\|\zeta_\varepsilon - \zeta\|_{W_0^1(\Omega)}^2 \leq C_1 \|\nabla(\zeta_\varepsilon - \zeta)\|_{L^2(\Omega)}^2, \quad (36)$$

From (35) and (36) we obtain

$$\|\zeta_\varepsilon - \zeta\|_{W_0^1(\Omega)}^2 \leq C_1 \left( \int_{B_\varepsilon(x^+)} (\zeta_\varepsilon - \zeta) \, dx - \int_{B_\varepsilon(x^-)} (\zeta_\varepsilon - \zeta) \, dx \right). \quad (37)$$

Therefore, thanks to the Cauchy-Schwarz inequality, there exist a constant  $C_2$  such that

$$\|\zeta_\varepsilon - \zeta\|_{W_0^1(\Omega)}^2 \leq C_2 \varepsilon \left( \|\zeta_\varepsilon - \zeta\|_{L^2(B_\varepsilon(x^+))} + \|\zeta_\varepsilon - \zeta\|_{L^2(B_\varepsilon(x^-))} \right). \quad (38)$$

Let  $\rho(x) = [\sqrt{1 + \|x\|^2} \log(2 + \|x\|^2)]^{-1}$ . Then  $0 < \rho(x) < 1$  for all  $x \in \Omega$ . Let us introduce  $\rho^* = \inf\{\rho(x), x \in B_{\varepsilon_0}(x^+) \cup B_{\varepsilon_0}(x^-)\}$  with the constant  $\varepsilon_0 > 0$ . Then, for any  $\varepsilon < \varepsilon_0$  we have

$$\begin{aligned} \|\zeta_\varepsilon - \zeta\|_{L^2(B_\varepsilon(x^+))} &\leq \frac{1}{\rho^*} \|\rho(\zeta_\varepsilon - \zeta)\|_{L^2(B_\varepsilon(x^+))} \\ &\leq \frac{1}{\rho^*} \|\rho(\zeta_\varepsilon - \zeta)\|_{L^2(\Omega)} \\ &\leq \frac{1}{\rho^*} \|\zeta_\varepsilon - \zeta\|_{W_0^1(\Omega)}, \end{aligned} \quad (39)$$

and

$$\|\zeta_\varepsilon - \zeta\|_{L^2(B_\varepsilon(x^-))} \leq \frac{1}{\rho^*} \|\zeta_\varepsilon - \zeta\|_{W_0^1(\Omega)}. \quad (40)$$

Then, from (38), (39) and (40) there exist a constant  $C_3$  such that

$$\|\zeta_\varepsilon - \zeta\|_{W_0^1(\Omega)}^2 \leq C_3 \varepsilon \|\zeta_\varepsilon - \zeta\|_{W_0^1(\Omega)}, \quad (41)$$

that can be expressed as

$$\|\zeta_\varepsilon - \zeta\|_{W_0^1(\Omega)} \leq C_3 \varepsilon. \quad (42)$$

On the other hand, from the Cauchy-Schwarz inequality and the trace theorem, we obtain

$$\left| \int_{\Gamma} (\zeta_\varepsilon - \zeta) \, ds \right| \leq C_4 |\Gamma| \|\zeta_\varepsilon - \zeta\|_{W_0^1(\Omega)}. \quad (43)$$

Therefore,

$$|c_\varepsilon - c| \leq C_4 \|\zeta_\varepsilon - \zeta\|_{W_0^1(\Omega)}. \quad (44)$$

Using (42), there exist a constant  $C_5$  such that

$$|c_\varepsilon - c| \leq C_5 \varepsilon. \quad (45)$$

Finally, since  $(\phi_\varepsilon - \phi) = (\zeta_\varepsilon - \zeta) + (c_\varepsilon - c)$ ,

$$\|\phi_\varepsilon - \phi\|_{W_0^1(\Omega)} \leq \|\zeta_\varepsilon - \zeta\|_{W_0^1(\Omega)} + |c_\varepsilon - c| \|1\|_{W_0^1(\Omega)}, \quad (46)$$

and using (42) and (45) we obtain (31) with  $C = C_3 + C_5 \|1\|_{W_0^1(\Omega)}$ .  $\square$

**Lemma 2.** *Let  $v$  and  $v_\varepsilon$  be solutions the the variational problems (24) and (30), respectively. Then, we have the following estimate for the difference  $v_\varepsilon - v$ ,*

$$\|v_\varepsilon - v\|_{W_0^1(\Omega)} \leq C \varepsilon, \quad (47)$$

where  $C$  is a constant independent of the small parameter  $\varepsilon$ .

*Proof.* According to (25), the solution of the adjoint problem can be obtained as  $v = w + \beta$  with  $w$  solution to the following variational problem

$$w \in V : \int_{\Omega} \nabla w \cdot \nabla \eta \, dx + \int_{\Gamma} \phi \eta \, ds = 0 \quad \forall \eta \in V, \quad (48)$$

and with the constant  $\beta = -|\Gamma| \int_{\Gamma} w \, ds$ . Analogously,  $v_\varepsilon = w_\varepsilon + \beta_\varepsilon$  with  $w_\varepsilon$  solution to the variational problem

$$w_\varepsilon \in V : \int_{\Omega} \nabla w_\varepsilon \cdot \nabla \eta \, dx + \int_{\Gamma} \phi_\varepsilon \eta \, ds = 0 \quad \forall \eta \in V, \quad (49)$$

and with the constant  $\beta_\varepsilon = -|\Gamma| \int_{\Gamma} w_\varepsilon \, ds$ . By subtracting the variational problems (48) and (49), we get

$$\int_{\Omega} \nabla(w_\varepsilon - w) \cdot \nabla \eta \, dx = \int_{\Gamma} (\phi_\varepsilon - \phi) \eta \, dx \quad \forall \eta \in V, \quad (50)$$

Now, by taking  $\eta = w_\varepsilon - w$ , we have

$$\int_{\Omega} \|\nabla(w_\varepsilon - w)\|^2 \, dx = \int_{\Gamma} (\phi_\varepsilon - \phi)(w_\varepsilon - w) \, dx. \quad (51)$$

Thanks to the behavior of  $(w_\varepsilon - w)$  at infinity, the Poincaré inequality gives [46]

$$\|w_\varepsilon - w\|_{W_0^1(\Omega)}^2 \leq C_1 \|\nabla(w_\varepsilon - w)\|_{L^2(\Omega)}^2, \quad (52)$$

From (51) and (52) we obtain

$$\|w_\varepsilon - w\|_{W_0^1(\Omega)}^2 \leq C_1 \int_{\Gamma} (\phi_\varepsilon - \phi)(w_\varepsilon - w) \, dx. \quad (53)$$

By taking into account the Cauchy-Schwarz inequality and the trace theorem, there exist a constan  $C_2$  such that

$$\begin{aligned} \|w_\varepsilon - w\|_{W_0^1(\Omega)}^2 &\leq C_1 \|\phi_\varepsilon - \phi\|_{H^{\frac{1}{2}}(\Gamma)} \|w_\varepsilon - w\|_{H^{\frac{1}{2}}(\Gamma)} \\ &\leq C_2 \|\phi_\varepsilon - \phi\|_{W_0^1(\Omega)} \|w_\varepsilon - w\|_{W_0^1(\Omega)}. \end{aligned} \quad (54)$$

Therefore, using Lemma 1, there exist  $C_3$  such that

$$\|w_\varepsilon - w\|_{W_0^1(\Omega)}^2 \leq C_3 \varepsilon \|w_\varepsilon - w\|_{W_0^1(\Omega)}, \quad (55)$$

which leads to

$$\|w_\varepsilon - w\|_{W_0^1(\Omega)} \leq C_3 \varepsilon. \quad (56)$$



In addition, from the Cauchy-Schwarz inequality and the trace theorem, we obtain

$$\left| \int_{\Gamma} (w_{\varepsilon} - w) ds \right| \leq C_4 |\Gamma| \|w_{\varepsilon} - w\|_{W_0^1(\Omega)}. \quad (57)$$

Therefore,

$$|\beta_{\varepsilon} - \beta| \leq C_4 \|w_{\varepsilon} - w\|_{W_0^1(\Omega)}. \quad (58)$$

From the result (56), there exist a constant  $C_5$  such that

$$|\beta_{\varepsilon} - \beta| \leq C_5 \varepsilon. \quad (59)$$

Finally, since  $(v_{\varepsilon} - v) = (w_{\varepsilon} - w) + (\beta_{\varepsilon} - \beta)$ ,

$$\|v_{\varepsilon} - v\|_{W_0^1(\Omega)} \leq \|w_{\varepsilon} - w\|_{W_0^1(\Omega)} + |\beta_{\varepsilon} - \beta| \|1\|_{W_0^1(\Omega)}, \quad (60)$$

and using (56) and (59) we obtain (47) with  $C = C_3 + C_5 \|1\|_{W_0^1(\Omega)}$ .  $\square$

Among the methods for calculation of the topological derivative currently available in literature, here we shall adopt the methodology developed in [47], which is given by the following result

$$D_T \psi = \lim_{\varepsilon \rightarrow 0} \frac{1}{f'(\varepsilon)} \frac{d}{d\varepsilon} \psi(\varepsilon), \quad (61)$$

where  $\frac{d}{d\varepsilon} \psi(\varepsilon)$  is the derivative of  $\psi(\varepsilon)$  with respect to the small parameter  $\varepsilon$ , which can be seen as the sensitivity of  $\psi(\varepsilon)$ , in the classical sense [19, 60] to the domain perturbation produced by an uniform expansion of the perturbation  $B_{\varepsilon}$ . Therefore, we can use the concept of shape sensitivity analysis as an intermediate step in the topological derivative calculation. This procedure enormously simplifies the analysis, allowing us to state the following result:

**Theorem 3.** *The topological derivative of the shape functional (15) is*

$$D_T \psi = -\mu_0 I (v(x^+) - v(x^-)). \quad (62)$$

Furthermore, the topological asymptotic expansion of the shape functional reads

$$\psi(\varepsilon) = \psi(0) - \pi \varepsilon^2 \mu_0 I (v(x^+) - v(x^-)) + o(\varepsilon^2). \quad (63)$$

*Proof.* The shape derivative of the functional (28) can be obtained as follows

$$\frac{d}{d\varepsilon} \psi(\varepsilon) = \dot{J}(\phi_{\varepsilon}) = \int_{\Gamma} \phi_{\varepsilon} \dot{\phi}_{\varepsilon} ds. \quad (64)$$

Now, let us calculate the shape derivative of the state equation (29), which leads to

$$\dot{\phi}_{\varepsilon} \in U : \int_{\Omega} \nabla \dot{\phi}_{\varepsilon} \cdot \nabla \eta dx = \frac{2}{\varepsilon} \mu_0 I \left( \int_{B_{\varepsilon}(x^+)} \eta dx - \int_{B_{\varepsilon}(x^-)} \eta dx \right) \quad \forall \eta \in U. \quad (65)$$

Since  $\dot{\phi}_{\varepsilon} \in U$ , we can take it as a test function in (30), namely  $\eta = \dot{\phi}_{\varepsilon}$ , to obtain

$$\int_{\Omega} \nabla v_{\varepsilon} \cdot \nabla \dot{\phi}_{\varepsilon} dx = - \int_{\Gamma} \phi_{\varepsilon} \dot{\phi}_{\varepsilon} ds. \quad (66)$$

In the same way, since  $v_{\varepsilon} \in U$ , we can take it as a test function in (29), namely  $\eta = v_{\varepsilon}$ , to obtain

$$\int_{\Omega} \nabla \dot{\phi}_{\varepsilon} \cdot \nabla v_{\varepsilon} dx = \frac{2}{\varepsilon} \mu_0 I \left( \int_{B_{\varepsilon}(x^+)} v_{\varepsilon} dx - \int_{B_{\varepsilon}(x^-)} v_{\varepsilon} dx \right). \quad (67)$$

By comparing both equations and taking into account the symmetry of the bilinear forms on their left-hand sides, we have from (64) the following important result

$$\dot{J}(\phi_{\varepsilon}) = -\frac{2}{\varepsilon} \mu_0 I \left( \int_{B_{\varepsilon}(x^+)} v_{\varepsilon} dx - \int_{B_{\varepsilon}(x^-)} v_{\varepsilon} dx \right). \quad (68)$$

In addition, by Lemma 2 we have

$$\|v_\varepsilon - v\|_{W_0^1(\Omega)} \leq C\varepsilon. \quad (69)$$

Therefore we can approximate  $v_\varepsilon$  as

$$v_\varepsilon(x) = v(x) + O(\varepsilon), \quad (70)$$

where  $v$  is solution to (24). Then, from the regularity of  $v$  at  $x^+$  and  $x^-$  we obtain

$$\begin{aligned} \frac{d}{d\varepsilon}\psi(\varepsilon) &= \dot{J}(\phi_\varepsilon) = -\frac{2}{\varepsilon}\mu_0 I (\pi\varepsilon^2 v(x^+) - \pi\varepsilon^2 v(x^-)) + O(\varepsilon^2) \\ &= -2\pi\varepsilon\mu_0 I (v(x^+) - v(x^-)) + O(\varepsilon^2). \end{aligned} \quad (71)$$

From the result (61) we obtain

$$D_T\psi = -\lim_{\varepsilon \rightarrow 0} \frac{2\pi\varepsilon}{f'(\varepsilon)} \mu_0 I (v(x^+) - v(x^-) + O(\varepsilon)). \quad (72)$$

Therefore, in order to extract the main term of the above expansion, we can choose  $f'(\varepsilon) = 2\pi\varepsilon$  ( $f(\varepsilon) = \pi\varepsilon^2$ ) and calculate the limit passage  $\varepsilon \rightarrow 0$  to obtain the desired result.  $\square$

Since we want to minimize the shape functional  $\psi$ , in the numerical approach we have to include a pair of inductors at the points  $x^+$  (positive inductor) and  $x^-$  (negative inductor) were the topological derivative  $D_T\psi$  takes its more negative values.

## 5. NUMERICAL METHOD

**5.1. The exterior Neumann problem.** We have seen that to compute the topological derivative given by formula (62) we have to solve the Neumann problems (20) and (23). To obtain approximate solutions for the these problems, we can resort again to functions  $\zeta$  and  $w$ , solutions to (18) and (25), respectively. So, let us consider the following general form of the exterior Neumann problem:

$$\begin{cases} -\Delta u = b & \text{in } \Omega, \\ \frac{\partial u}{\partial n} = q & \text{on } \Gamma, \\ u(x) = o(1) & \text{as } \|x\| \rightarrow \infty, \end{cases} \quad (73)$$

The solution  $u$  of (73) satisfies the following integral equation [8, 35, 13, 12]

$$c(\xi)u(\xi) + \int_\Gamma q^*(\xi, x)u \, d\gamma - \int_\Gamma u^*(\xi, x)q(x) \, d\gamma = \int_\Omega u^*(\xi, x)b(x) \, dx, \quad (74)$$

where  $u^*$  is the fundamental solution of the problem,  $u^*(\xi, x) = -\frac{1}{2\pi} \log \|\xi - x\|$ ,  $q^*(\xi, x) = \frac{\partial u^*}{\partial n}(\xi, x)$ , the characteristic function  $c(\xi) = 1$ , for any interior point  $\xi$ , and  $c(\xi) = \frac{\Delta\theta}{2\pi}$ , for any point  $\xi \in \Gamma$ , where  $\Delta\theta$  is the angle, internal to  $\Omega$ , formed by the right and left tangents to  $\Gamma$  at  $\xi$  ( $c(\xi) = \frac{1}{2}$  at points where  $\Gamma$  is smooth). The first integral on left hand side of (74) must be understood in the Cauchy principal value sense.

The spatial discretization consists in approximating the boundary  $\Gamma$  into  $N$  linear elements  $\Gamma_j$ ,  $1 \leq j \leq N$ . The functions  $u$  and  $q$  are approximated inside each element by piecewise linear polynomials in the form:

$$u(x) = \mathbf{N}(x)\mathbf{u}^{(j)}, \quad q(x) = \mathbf{N}(x)\mathbf{q}^{(j)}, \quad \text{in } \Gamma_j, \quad (75)$$

where  $\mathbf{N}$  is the  $1 \times 2$  matrix of the linear interpolation functions and  $\mathbf{u}^{(j)}$  and  $\mathbf{q}^{(j)}$  are the vectors that contain the nodal variables corresponding to  $u$  and  $q$  in the element  $\Gamma_j$ . The collocation boundary element method (BEM), builds a linear system imposing (74) at each node  $\xi_i$  of the boundary:

$$c_i u_i + \sum_{j=1}^N \mathbf{h}_{ij} \mathbf{u}^{(j)} - \sum_{j=1}^N \mathbf{g}_{ij} \mathbf{q}^{(j)} = u_1(\xi_i), \quad 1 \leq i \leq N, \quad (76)$$

where the element matrices  $\mathbf{h}_{ij}$  and  $\mathbf{g}_{ij}$  are:

$$\mathbf{h}_{ij} = \int_{\Gamma_j} q^*(\xi, x) \mathbf{N}(x) d\gamma, \quad \mathbf{g}_{ij} = \int_{\Gamma_j} u^*(\xi, x) \mathbf{N}(x) d\gamma, \quad (77)$$

and the function  $u_1$ , which is a particular solution of (73), is defined as:

$$u_1(\xi) = \int_{\Omega} u^*(\xi, x) b(x) dx. \quad (78)$$

The linear system (76) can be expressed in matrix form as:

$$\mathbf{H}\mathbf{u} = \mathbf{G}\mathbf{q} + \mathbf{u}_1, \quad (79)$$

where  $\mathbf{H}$  was assembled from the values of  $c_i$  and  $\mathbf{h}_{ij}$ ,  $\mathbf{G}$  from the values of matrices  $\mathbf{g}_{ij}$ , the vectors  $\mathbf{u}$  and  $\mathbf{q}$  contain all the nodal variables corresponding to  $u$  and  $q$ , respectively, and  $(\mathbf{u}_1)_i = u_1(\xi_i)$ .

Once solved the linear system (79), the solution  $\mathbf{u}$  provides the piecewise approximation of  $u$  on  $\Gamma$  by using (75). The approximate solution at interior points is obtained using (74), with  $c(\xi) = 1$ , and with  $u$  and  $q$  defined on  $\Gamma$  by the interpolation expressions of (75).

**5.2. Construction of the solution.** The numerical algorithm will look for a current distribution  $j_0$  of the form:

$$j_0 = I \sum_{p=1}^m \alpha_p \chi_{\Theta_p}, \quad (80)$$

where  $I$  is a predefined intensity of current, the cells  $\Theta_p$ , with  $1 \leq p \leq m$ , are fixed bounded domains,  $\chi_{\Theta_p}$  are their characteristic functions, and  $\alpha_p \in \{-1, 0, 1\}$ . The solution of the design problem will be constructed changing the values of  $\alpha_p$ . Note that the expression (80) assumes that the electric current density is uniform on each cell  $\Theta_p$ . Inductors made of bundled insulated strands allow the use of (80) as a good approximation, see [61] and references therein.

Before starting with the optimization process, we have to define a mesh of linear elements approximating the boundary  $\Gamma$ , and the mesh of cells  $\Theta_p$  in a region inside  $\Omega$  surrounding the liquid metal. For each of these cells we have to set the initial value for the parameters  $\alpha_p$  of (80). If there is no information about what would be a good initial configuration, the value  $\alpha_p = 0$  should be chosen. The value of the constant  $p_0$  must be computed using (12). For numerical calculations, the curvature  $\mathcal{C}$  at a node of the boundary mesh is approximated by the curvature of the circumference defined by it and adjacent nodes. Inside the elements the curvature is linearly interpolated. Next we have to define the function  $\varkappa = \pm 1$  with a sign change at each global maximum of the piecewise approximation of the curvature. Curves for which this definition of  $\varkappa$  does not satisfies the compatibility condition (17), or having an odd number of global maximum points, are strictly not shapable. However, some extra sign changes can be defined in order to have (17) satisfied. Some examples of application of this technique to obtain an approximate solution for curves that are not shapable are shown in Section 6. Finally, we have to assign a power of two to the integer variable NC. NC is the variable that determines how many cells increase and how many decrease the value of the electric current density at each iteration.

The procedure proposed here to build the solution is the following:

- (1) Find  $\phi$  on the boundary by solving the exterior Neumann problem (16) and compute the initial value of the objective function  $J(\phi)$ .
- (2) Find the adjoint state  $v$  on the boundary by solving the exterior Neumann problem (23) and compute it at the center of each cell of the mesh.
- (3) For the set of cells with  $\alpha_p \leq 0$ , set  $\alpha_p := \alpha_p + 1$  to the NC cells that have the largest values of  $v$ . For the set of cells with  $\alpha_p \geq 0$ , set  $\alpha_p := \alpha_p - 1$  to the NC cells that have the smallest values of  $v$ .

- (4) Solve the exterior Neumann problem (16) on the boundary and compute the new value of the objective function  $J(\phi)$ . If the objective function has decreased then return to step (2). Otherwise, undo the changes made in step (3) and set  $NC := NC/2$ . If  $NC < 1$  stop. Otherwise, return to step (3).

Note that the previous procedure generates a sequence of solutions that monotonically decrease the value of the objective function. Note also that the stopping criterium is the most rigorous possible, because the procedure stops only if it can not find other solution having a smaller value of the objective function.

Step (2) is by far the most expensive of the previous procedure. Roughly speaking, the number of operations of this step is proportional to the number of elements of the boundary mesh times the number of cells of the domain mesh. The number of operations of steps (1) and (4) is related only to the number of elements of the boundary mesh. The number of operations of step (3) is also related to the number of cells of the domain mesh, but the ordering operations of this step can be performed in significantly less time than the operations of step (2).

## 6. NUMERICAL EXAMPLES

6.1. **Example 1.** The target shape of this example is the solution of a direct free-surface problem for a liquid metal column of cross-section area  $S_0 = \pi$ , considering four distributed currents of density  $I = 0.5$  as shown in Fig. 1. The surface tension  $\sigma = 1.0 \times 10^{-4}$  and  $\mu_0 = 1.0$ . For the inverse problem we considered two cases, named Ex1a and Ex1b, for meshes of cells of size  $D = 0.05$  and  $D = 0.02$  respectively, defined in the region shown in Fig. 1. As well as in the next examples, the initial value  $\alpha_p = 0$  was taken for all the cells. The results obtained are shown in Fig. 2. The evolution of the objective function along the iterative process is shown in Fig. 3.

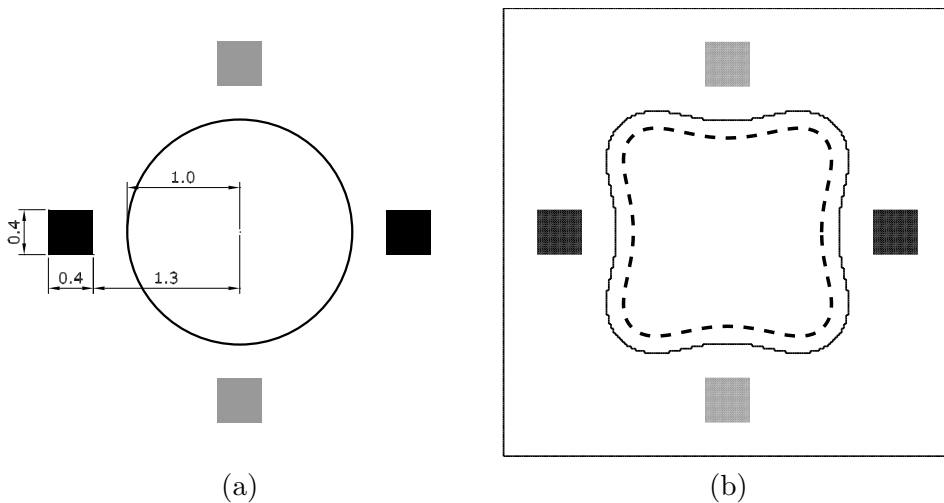


FIGURE 1. Example 1. (a) Initial configuration of the direct free-surface problem. (b) Target shape and exact solution. Black area: positive inductors, gray area: negative inductors, dashed line: target shape, thin solid line: boundary of the mesh of cells.

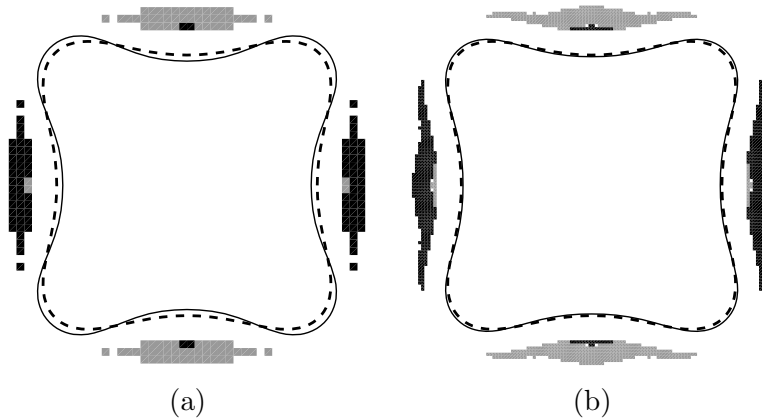


FIGURE 2. Example 1. (a) Solution for a mesh of cells of size  $D = 0.05$ . (b) Solution for a mesh of cells of size  $D = 0.02$ . Black area: positive inductors, gray area: negative inductors, dashed line: target shape, thin solid line: equilibrium shape.

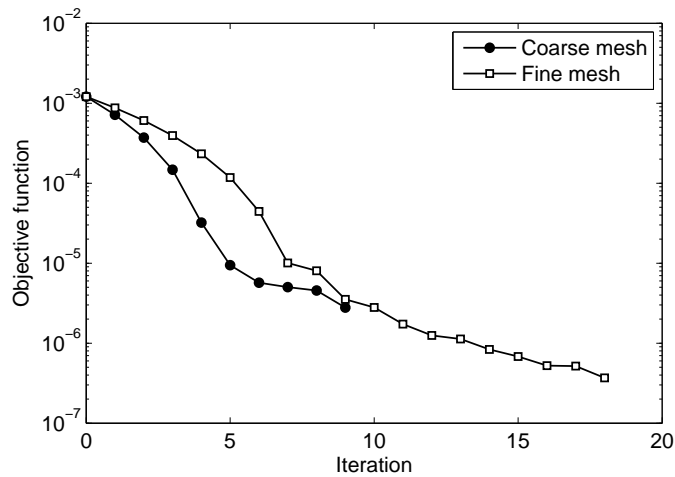


FIGURE 3. Example 1. Evolution of the objective function.

6.2. **Example 2.** This example is similar to the previous one, with the difference that six distributed currents of density  $I = 0.4$  were considered for the direct free-surface problem as shown in Fig. 4. Two cases, named Ex2a and Ex2b, for meshes of cells of size  $D = 0.05$  and  $D = 0.02$  respectively, defined in the region shown in Fig. 4 were considered. The results obtained are shown in Fig. 5. The evolution of the objective function along the iterative process is shown in Fig. 6.

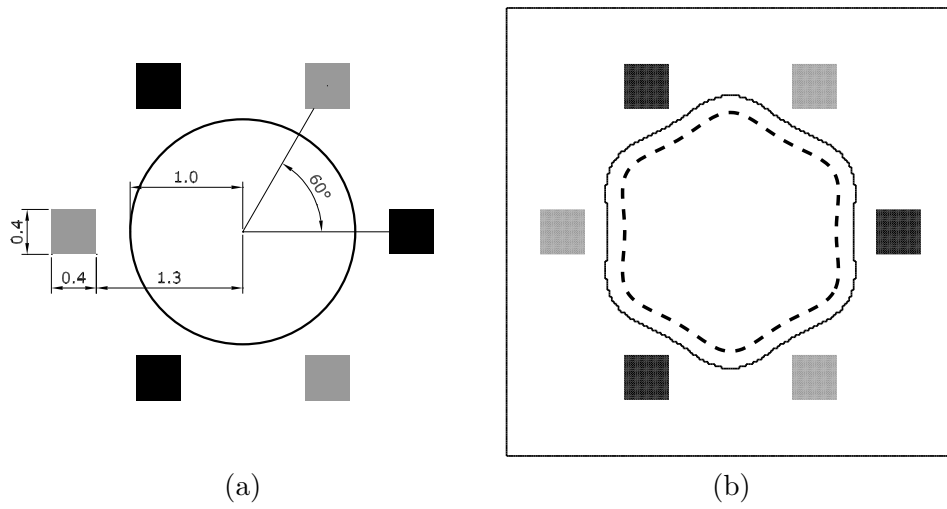


FIGURE 4. Example 2. (a) Initial configuration of the direct free-surface problem. (b) Target shape and exact solution. Black area: positive inductors, gray area: negative inductors, dashed line: target shape, thin solid line: boundary of the mesh of cells.

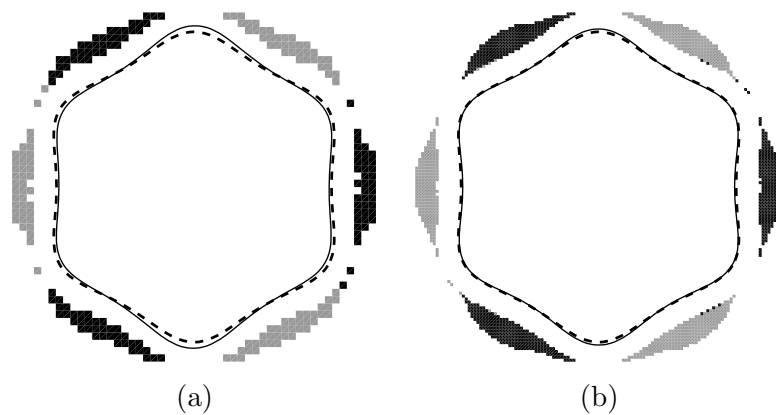


FIGURE 5. Example 2. (a) Solution for a mesh of cells of size  $D = 0.05$ . (b) Solution for a mesh of cells of size  $D = 0.02$ . Black area: positive inductors, gray area: negative inductors, dashed line: target shape, thin solid line: equilibrium shape.

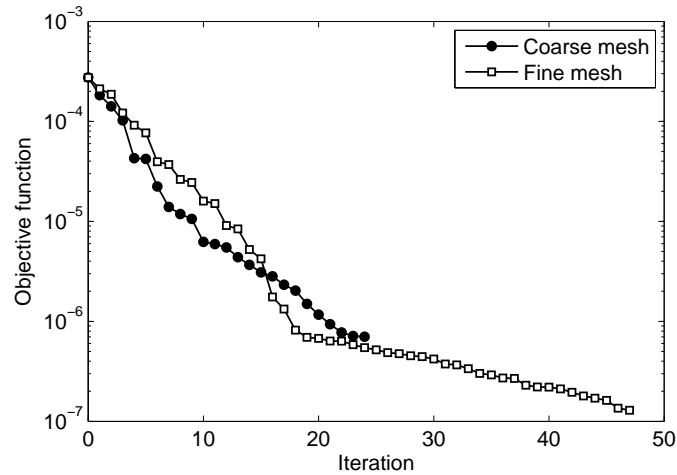


FIGURE 6. Example 2. Evolution of the objective function.

**6.3. Example 3.** The target shape of this example is the round rectangle depicted in Fig. 7. The current density  $I = 0.2$ ,  $\sigma = 1.0 \times 10^{-4}$  and  $\mu_0 = 1.0$ . Two cases, named Ex3a and Ex3b, for meshes of cells of size  $D = 0.05$  and  $D = 0.02$  respectively, defined in the region shown in Fig. 7 were considered. For this example, the compatibility equation (17) is not satisfied if the sign changes of  $\varkappa$  are defined just at the four vertices of the rectangle. However, the compatibility holds if we define two extra sign changes at locations shown in Fig. 7. For this case, the results obtained are shown in Fig. 8. The evolution of the objective function along the iterative process is shown in Fig. 9.

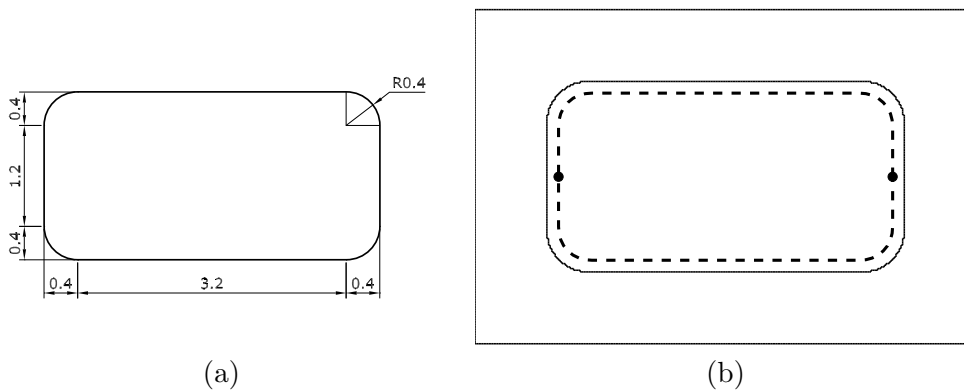


FIGURE 7. Example 3. (a) Description of the problem geometry. (b) Target shape. Dashed line: target shape, thin solid line: boundary of the mesh of cells, black dots: location of the two extra sign changes of  $\varkappa$ .

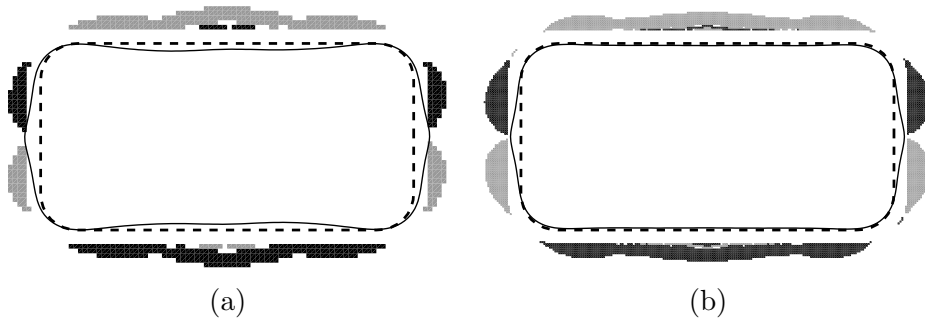


FIGURE 8. Example 3. (a) Solution for a mesh of cells of size  $D = 0.05$ . (b) Solution for a mesh of cells of size  $D = 0.02$ . Black area: positive inductors, gray area: negative inductors, dashed line: target shape, thin solid line: equilibrium shape.

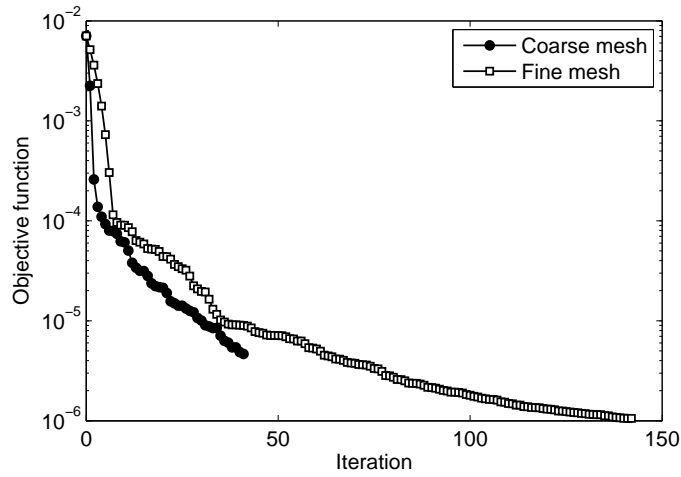


FIGURE 9. Example 3. Evolution of the objective function.

6.4. **Example 4.** The target shape of this example is depicted in Fig. 10. The current density  $I = 0.2$ ,  $\sigma = 1.0 \times 10^{-4}$  and  $\mu_0 = 1.0$ . Two cases, named Ex4a and Ex4b, for meshes of cells of size  $D = 0.05$  and  $D = 0.02$  respectively, defined in the region shown in Fig. 10 were considered. The results obtained are shown in Fig. 11. The evolution of the objective function along the iterative process is shown in Fig. 12.



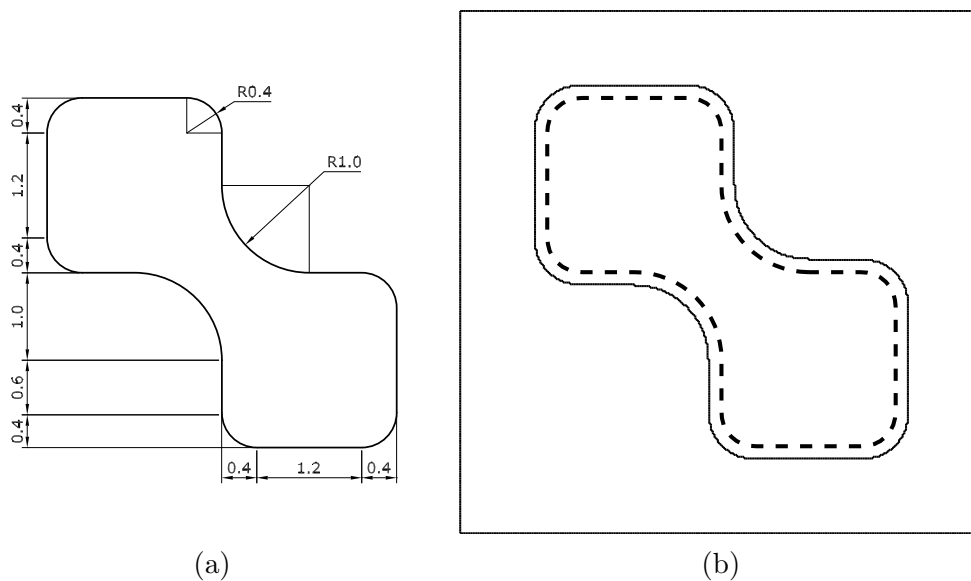


FIGURE 10. Example 4. (a) Description of the problem geometry. (b) Target shape. Dashed line: target shape, thin solid line: boundary of the mesh of cells.

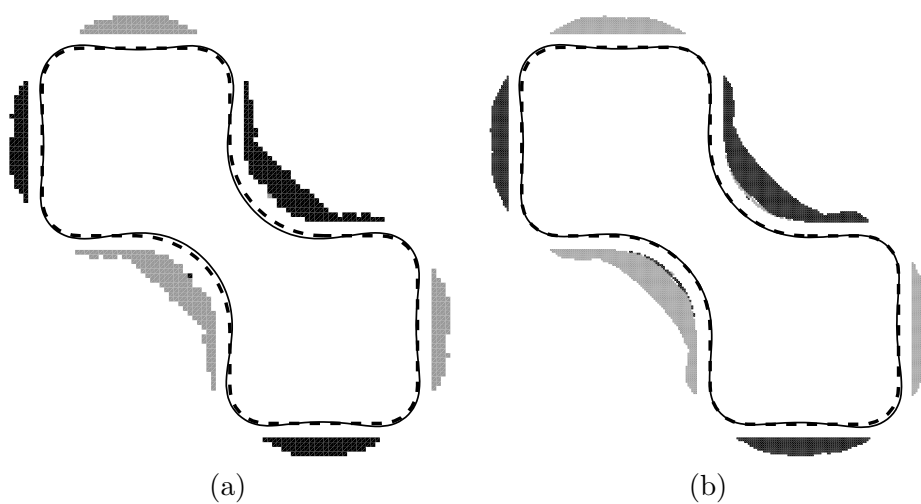


FIGURE 11. Example 4. (a) Solution for a mesh of cells of size  $D = 0.05$ . (b) Solution for a mesh of cells of size  $D = 0.02$ . Black area: positive inductors, gray area: negative inductors, dashed line: target shape, thin solid line: equilibrium shape.

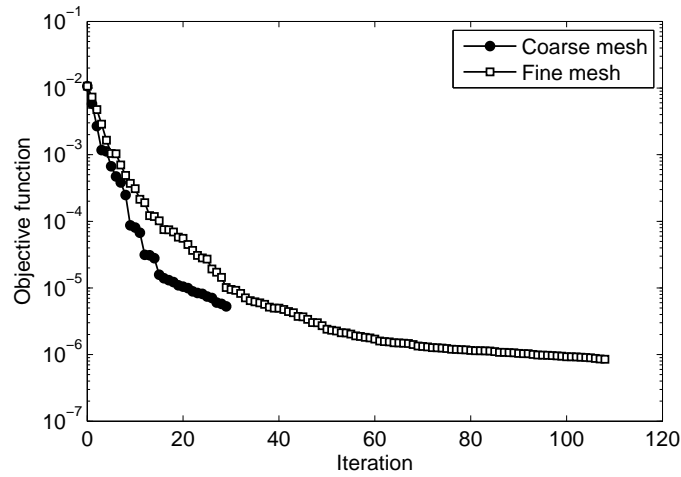


FIGURE 12. Example 4. Evolution of the objective function.

6.5. **Example 5.** The target shape of this example is depicted in Fig. 13. The current density  $I = 0.2$ ,  $\sigma = 1.0 \times 10^{-4}$  and  $\mu_0 = 1.0$ . Two cases, named Ex5a and Ex5b, for meshes of cells of size  $D = 0.05$  and  $D = 0.02$  respectively, defined in the region shown in Fig. 13 were considered. As well as in the Example 3, the function  $\varkappa$  was defined with two extra sign changes with the purpose of satisfying the compatibility equation. The results obtained are shown in Fig. 14. The evolution of the objective function along the iterative process is shown in Fig. 15.

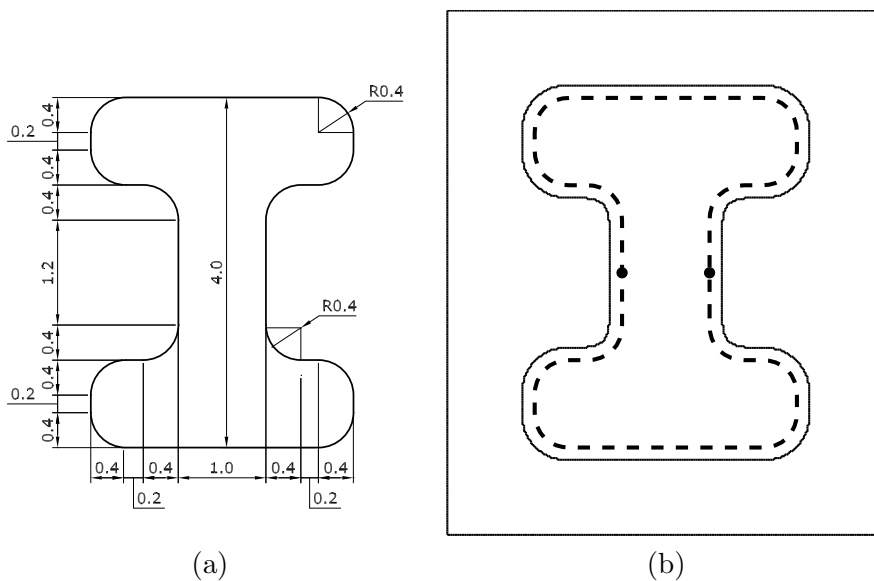


FIGURE 13. Example 5. (a) Description of the problem geometry. (b) Target shape. Dashed line: target shape, thin solid line: boundary of the mesh of cells, black dots: location of the two extra sign changes of  $\varkappa$ .

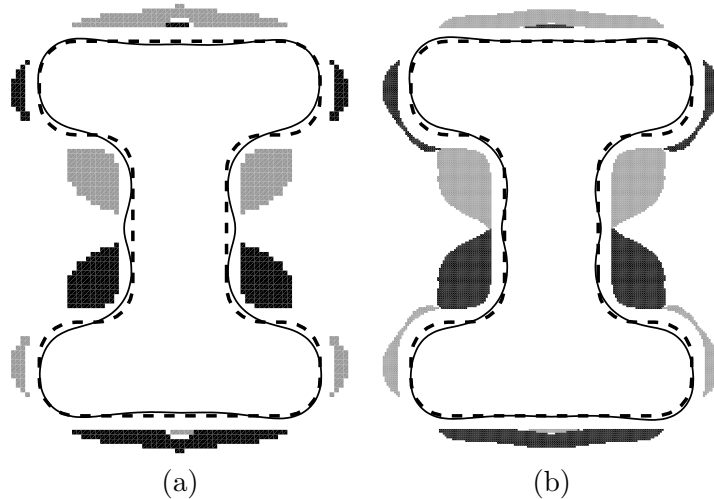


FIGURE 14. Example 5. (a) Solution for a mesh of cells of size  $D = 0.05$ . (b) Solution for a mesh of cells of size  $D = 0.02$ . Black area: positive inductors, gray area: negative inductors, dashed line: target shape, thin solid line: equilibrium shape.

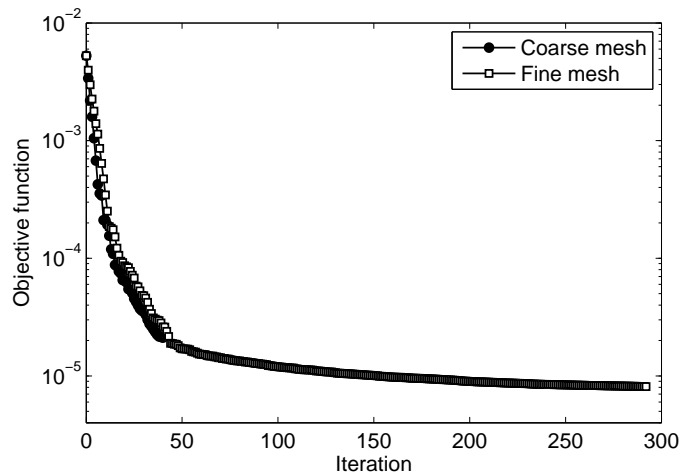


FIGURE 15. Example 5. Evolution of the objective function.

**6.6. Results summary.** Table 1 resumes the information about the considered examples. For each one the number of iterations performed by the optimization algorithm is indicated as well as the final value of the objective function. Note that the target shapes of examples 1 to 2 are solutions of direct free-surface problems considering known electric currents. Then, those currents constitute exact solutions for the inverse problem considered here. However, as shown in the previous figures, the inductors obtained by the optimization algorithm are clearly different from the known exact solutions. This fact, instead of indicating that the algorithm did not work properly, suggests that the inductor design problem have multiple solutions. Table 1 shows that, for these examples, the optimization algorithm obtained approximated solutions with the value of the total intensity of current clearly lower than the associated to the known exact solutions. Thus, the results obtained suggest the idea that the optimization algorithm looks for an economic design, which is consistent with the idea that inspires the use of the topological derivative: the algorithm puts inductors in the location where they produce the largest influence on the shape functional.

Examples 3 to 5 show that the proposed approach is also effective dealing with truly inverse problems defined considering general shapes. The best result was obtained for the Example 4, which, because of the especial symmetry of the problem, exactly satisfies the compatibility equation (17). The examples 3 and 5 required the definition of  $\varkappa$  with some extra sign changes to satisfy the compatibility equation. For these examples, the results of the free-surface problem show that the equilibrium shapes have points of maximum curvature in places where they should not be. The equilibrium shapes obtained for these examples are, however, quite close to the target shapes.

TABLE 1. Results summary.

Example	NE	TC	NC	Iter	II	IS	IOF	FOF
Ex1a	128	4692	16	9	0.160	0.110	1.209e-03	2.779e-06
Ex1b	128	29304	64	18	0.160	0.118	1.209e-03	3.681e-07
Ex2a	120	4724	16	24	0.192	0.112	2.747e-04	7.013e-07
Ex2b	120	29520	64	47	0.192	0.109	2.747e-04	1.292e-07
Ex3a	120	5744	32	42	–	0.143	7.059e-03	4.691e-06
Ex3b	120	36128	128	142	–	0.160	7.059e-03	1.056e-06
Ex4a	152	10228	32	29	–	0.161	1.066e-02	5.300e-06
Ex4b	152	64120	128	108	–	0.173	1.066e-02	8.523e-07
Ex5a	180	7864	32	40	–	0.216	5.258e-03	2.113e-05
Ex5b	180	49368	128	292	–	0.264	5.258e-03	8.129e-06

NE: number of elements, TC: total number of cells, NC: initial number of cells that are selected to change the sign, Iter: number of iterations performed, II: total intensity of the positive inductors of the known exact solution. IS: total intensity of the positive inductors of the solution obtained, IOF: initial value of the objective function, FOF: final value of the objective function.

## 7. CONCLUSIONS

In this paper we have described a new method for the topology design of inductors in electromagnetic casting. For the two-dimensional case, a new formulation of the design problem based on the Kohn-Vogelius functional was stated. The topological derivative of the Kohn-Vogelius functional regarding the introduction of small inductors was derived. A numerical procedure that makes use of the topological derivative to construct the solution was proposed.

Some examples presented show that the method proposed is effective to design suitable inductors. For some examples with known exact solutions, the method was able to obtain solutions with a value of the total intensity of current clearly lower than the associated to the known solution. This fact suggests that the use of topological derivatives provides the proposed method with the intrinsic ability of obtaining the most economical design, with respect to the total intensity of current, among those belonging to the set of solutions. Some other examples with unknown solutions were also successfully solved.

In summary, the method proposed is easy to code and can be successfully used in the design of inductors in electromagnetic casting, considering general geometries as objective.

## ACKNOWLEDGEMENTS

The authors thank the Brazilian Research Councils CAPES, CNPq and FAPERJ, the Uruguayan National Research and Innovation Agency (ANII) and the French Research Councils COFECUB, INRIA and CNRS for the financial support.

## REFERENCES

- [1] G. Allaire, F. de Gournay, F. Jouve, and A.-M. Toader. Structural optimization using topological and shape sensitivity via a level set method. *Control and Cybernetics*, 34(1):59–80, 2005.
- [2] S. Amstutz. Sensitivity analysis with respect to a local perturbation of the material property. *Asymptotic Analysis*, 49(1-2):87–108, 2006.
- [3] S. Amstutz and H. Andrä. A new algorithm for topology optimization using a level-set method. *Journal of Computational Physics*, 216(2):573–588, 2006.
- [4] S. Amstutz, S. M. Giusti, A. A. Novotny, and E. A. de Souza Neto. Topological derivative in multi-scale linear elasticity models applied to the synthesis of microstructures. *International Journal for Numerical Methods in Engineering*, 84(6):733–756, 2010.
- [5] S. Amstutz, I. Horchani, and M. Masmoudi. Crack detection by the topological gradient method. *Control and Cybernetics*, 34(1):81–101, 2005.
- [6] S. Amstutz and A. A. Novotny. Topological asymptotic analysis of the Kirchhoff plate bending problem. *ESAIM. Control, Optimisation and Calculus of Variations*, Online, 2010.
- [7] S. Amstutz and A. A. Novotny. Topological optimization of structures subject to von Mises stress constraints. *Structural and Multidisciplinary Optimization*, 41(3):407–420, 2010.
- [8] K. E. Atkinson. *The numerical solution of integral equations of the second kind*, volume 4 of *Cambridge Monographs on Applied and Computational Mathematics*. Cambridge University Press, Cambridge, 1997.
- [9] D. Auroux, M. Masmoudi, and L. Belaid. Image restoration and classification by topological asymptotic expansion. In E. Taroco, E. A. de Souza Neto, and A. A. Novotny, editors, *Variational formulations in mechanics: theory and applications*, Barcelona, Spain, 2007.
- [10] L. J. Belaid, M. Jaoua, M. Masmoudi, and L. Siala. Application of the topological gradient to image restoration and edge detection. *Engineering Analysis with Boundary Elements*, 32(11):891–899, 2008.
- [11] J.-P. Brancher and O. E. Séro-Guillaume. Étude de la déformation d’un liquide magnétique. *Archive for Rational Mechanics and Analysis*, 90(1):57–85, 1985.
- [12] C. A. Brebbia and J. Dominguez. *Boundary elements: an introductory course*. Computational Mechanics Publications, Southampton, second edition, 1992.
- [13] C. A. Brebbia, J. C. F. Telles, and L. C. Wrobel. *Boundary Element Technique: Theory and Applications in Engineering*. Springer-Verlag, 1984.
- [14] M. Brühl, M. Hanke, and M. S. Vogelius. A direct impedance tomography algorithm for locating small inhomogeneities. *Numerische Mathematik*, 93(4):635–654, 2003.
- [15] M. Burger, B. Hackl, and W. Ring. Incorporating topological derivatives into level set methods. *Journal of Computational Physics*, 194(1):344–362, 2004.
- [16] A. Canelas, J. R. Roche, and J. Herskovits. Inductor shape optimization for electromagnetic casting. *Structural and Multidisciplinary Optimization*, 39(6):589–606, 2009.
- [17] A. Canelas, J. R. Roche, and J. Herskovits. The inverse electromagnetic shaping problem. *Structural and Multidisciplinary Optimization*, 38(4):389–403, 2009.
- [18] J. R. de Faria and A. A. Novotny. On the second order topological asymptotic expansion. *Structural and Multidisciplinary Optimization*, 39(6):547–555, 2009.
- [19] M. C. Delfour and J.-P. Zolésio. *Shapes and geometries*, volume 4 of *Advances in Design and Control*. Society for Industrial and Applied Mathematics (SIAM), Philadelphia, PA, 2001. Analysis, differential calculus, and optimization.
- [20] K. Eppler and H. Harbrecht. On a kohn-vogelius like formulation of free boundary problems. *Computational Optimization and Applications*, Online, 2010.
- [21] G. R. Feijóo. A new method in inverse scattering based on the topological derivative. *Inverse Problems*, 20(6):1819–1840, 2004.
- [22] T. P. Felici and J.-P. Brancher. The inverse shaping problem. *European Journal of Mechanics. B Fluids*, 10(5):501–512, 1991.
- [23] G. Frémiot, W. Horn, A. Laurain, M. Rao, and J. Sokolowski. On the analysis of boundary value problems in nonsmooth domains. *Dissertationes Mathematicae (Rozprawy Matematyczne)*, 462:149, 2009.
- [24] A. Friedman and M. Vogelius. Identification of small inhomogeneities of extreme conductivity by boundary measurements: a theorem on continuous dependence. *Archive for Rational Mechanics and Analysis*, 105(4):299–326, 1989.
- [25] H. Z. Fu, J. Shen, L. Liu, Q. T. Hao, S. M. Li, and J. S. Li. Electromagnetic shaping and solidification control of Ni-base superalloys under vacuum. *Journal of Materials Processing Technology*, 148(1):25–29, 2004.
- [26] A. Gagnoud, J. Etay, and M. Garnier. Le problème de frontière libre en lévitation électromagnétique. *Journal de Mécanique Théorique et Appliquée*, 5(6):911–934, 1986.
- [27] S. Garreau, P. Guillaume, and M. Masmoudi. The topological asymptotic for PDE systems: the elasticity case. *SIAM Journal on Control and Optimization*, 39(6):1756–1778, 2001.
- [28] B. B. Guzina and M. Bonnet. Small-inclusion asymptotic of misfit functionals for inverse problems in acoustics. *Inverse Problems*, 22(5):1761–1785, 2006.

- [29] A. Henrot, J.-P. Brancher, and M. Pierre. Existence of equilibria in electromagnetic casting. In *Proceedings of the Fifth International Symposium on Numerical Methods in Engineering, Vol. 1, 2 (Lausanne, 1989)*, pages 221–228, Southampton, 1989. Comput. Mech.
- [30] A. Henrot and M. Pierre. Un problème inverse en formage des métaux liquides. *RAIRO Modélisation Mathématique et Analyse Numérique*, 23(1):155–177, 1989.
- [31] M. Hintermüller. Fast level set based algorithms using shape and topological sensitivity information. *Control and Cybernetics*, 34(1):305–324, 2005.
- [32] M. Hintermüller and A. Laurain. Electrical impedance tomography: from topology to shape. *Control and Cybernetics*, 37(4):913–933, 2008.
- [33] M. Hintermüller and A. Laurain. Multiphase image segmentation and modulation recovery based on shape and topological sensitivity. *Journal of Mathematical Imaging and Vision*, 35:1–22, 2009.
- [34] I. Hlaváček, A. A. Novotny, J. Sokołowski, and A. Żochowski. On topological derivatives for elastic solids with uncertain input data. *Journal of Optimization Theory and Applications*, 141(3):569–595, 2009.
- [35] G. Hsiao and W. L. Wendland. *Boundary Integral Equations*, volume 164 of *Applied Mathematical Sciences*. Springer-Verlag, Berlin, 2008.
- [36] A. M. Khludnev, A. A. Novotny, J. Sokołowski, and A. Żochowski. Shape and topology sensitivity analysis for cracks in elastic bodies on boundaries of rigid inclusions. *Journal of the Mechanics and Physics of Solids*, 57(10):1718–1732, 2009.
- [37] R. Kohn and M. Vogelius. Determining conductivity by boundary measurements. *Communications on Pure and Applied Mathematics*, 37(3):289–298, 1984.
- [38] I. Larrabide, R. A. Feijóo, A. A. Novotny, and E. Taroco. Topological derivative: a tool for image processing. *Computers & Structures*, 86(13-14):1386–1403, 2008.
- [39] T. Lewiński and J. Sokołowski. Energy change due to the appearance of cavities in elastic solids. *International Journal of Solids and Structures*, 40(7):1765–1803, 2003.
- [40] M. Masmoudi, J. Pommier, and B. Samet. The topological asymptotic expansion for the Maxwell equations and some applications. *Inverse Problems*, 21(2):547–564, 2005.
- [41] H. K. Moffatt. Magnetostatic equilibria and analogous Euler flows of arbitrarily complex topology. Part 1. Fundamentals. *Journal of Fluid Mechanics*, 159:359–378, 1985.
- [42] S. A. Nazarov and J. Sokołowski. Asymptotic analysis of shape functionals. *Journal de Mathématiques Pures et Appliquées*, 82(2):125–196, 2003.
- [43] S. A. Nazarov and J. Sokołowski. Self adjoint extensions of differential operators in application to shape optimization. *Comptes Rendus Mécanique*, 331(10):667–672, 2003.
- [44] S. A. Nazarov and J. Sokołowski. Singular perturbations in shape optimization for the Dirichlet Laplacian. *Comptes Rendus Mécanique*, 333(4):305–310, 2005.
- [45] S. A. Nazarov and J. Sokołowski. Self-adjoint extensions for the Neumann Laplacian and applications. *Acta Mathematica Sinica*, 22(3):879–906, 2006.
- [46] J.-C. Nédélec. *Acoustic and Electromagnetic Equations. Integral Representations for Harmonic Problems*, volume 144 of *Applied Mathematical Sciences*. Springer-Verlag, New York, 2001.
- [47] A. A. Novotny, R. A. Feijóo, E. Taroco, and C. Padra. Topological sensitivity analysis. *Computer Methods in Applied Mechanics and Engineering*, 192(7-8):803–829, 2003.
- [48] A. A. Novotny, R. A. Feijóo, E. Taroco, and C. Padra. Topological sensitivity analysis for three-dimensional linear elasticity problem. *Computer Methods in Applied Mechanics and Engineering*, 196(41-44):4354–4364, 2007.
- [49] A. Novruzi and J. R. Roche. Second order derivatives, Newton method, application to shape optimization. Technical Report RR-2555, INRIA, 1995.
- [50] A. Novruzi and J. R. Roche. Newton’s method in shape optimisation: A three-dimensional case. *BIT. Numerical Mathematics*, 40(1):102–120, 2000.
- [51] M. Pierre and J. R. Roche. Computation of free surfaces in the electromagnetic shaping of liquid metals by optimization algorithms. *European Journal of Mechanics. B Fluids*, 10(5):489–500, 1991.
- [52] M. Pierre and J. R. Roche. Numerical simulation of tridimensional electromagnetic shaping of liquid metals. *Numerische Mathematik*, 65(1):203–217, 1993.
- [53] J. R. Roche. Gradient of the discretized energy method and discretized continuous gradient in electromagnetic shaping simulation. *Applied Mathematics and Computer Science*, 7(3):545–565, 1997.
- [54] J. R. Roche. Adaptive Newton-like method for shape optimization. *Control and Cybernetics*, 34(1):363–377, 2005.
- [55] J. R. Roche and J. Sokołowski. Numerical methods for shape identification problems. *Control and Cybernetics*, 25(5):867–894, 1996. Shape optimization and scientific computations (Warsaw, 1995).
- [56] J. A. Shercliff. Magnetic shaping of molten metal columns. *Proceedings of the Royal Society of London. Series A, Mathematical and Physical Sciences*, 375(1763):455–473, 1981.
- [57] J. Sokołowski and A. Żochowski. On the topological derivative in shape optimization. *SIAM Journal on Control and Optimization*, 37(4):1251–1272, 1999.

- [58] J. Sokołowski and A. Żochowski. Optimality conditions for simultaneous topology and shape optimization. *SIAM Journal on Control and Optimization*, 42(4):1198–1221, 2003.
- [59] J. Sokołowski and A. Żochowski. Modelling of topological derivatives for contact problems. *Numerische Mathematik*, 102(1):145–179, 2005.
- [60] J. Sokołowski and J.-P. Zolésio. *Introduction to shape optimization*, volume 16 of *Springer Series in Computational Mathematics*. Springer-Verlag, Berlin, 1992. Shape sensitivity analysis.
- [61] C. R. Sullivan. Optimal choice for number of strands in a litz-wire transformer winding. *IEEE Transactions On Power Electronics*, 14(2):283–291, 1999.
- [62] C. Zhiqiang, J. Fei, Z. Xingguo, H. Hai, and J. Junze. Microstructures and mechanical characteristics of electromagnetic casting and direct-chill casting 2024 aluminum alloys. *Materials Science and Engineering A*, 327(2):133–137, 2002.

(Canelas) INSTITUTO DE ESTRUCTURAS Y TRANSPORTE, FACULTAD DE INGENIERÍA, UDELAR, J. HERRERA Y REISSIG 565, CP 11300, MONTEVIDEO, URUGUAY  
*E-mail address:* `acanelas@fing.edu.uy`

(Novotny) LABORATÓRIO NACIONAL DE COMPUTAÇÃO CIENTÍFICA LNCC/MCT, AV. GETÚLIO VARGAS 333, 25651-075, PETRÓPOLIS - RJ, BRASIL  
*E-mail address:* `novotny@lncc.br`

(Roche) INSTITUT ELIE CARTAN DE NANCY, NANCY-UNIVERSITÉ, CNRS, INRIA, B.P. 70239, 54506, VANDOEUVRE LÈS NANCY, FRANCE  
*E-mail address:* `roche@iecn.u-nancy.fr`